Publication Year	2022
Acceptance in OA	2023-01-23T10:28:42Z
Title	Theoretical Estimate of the Half-life for the Radioactive 134Cs and 135Cs in Astrophysical Scenarios
Authors	Taioli, Simone, VESCOVI, DIEGO, Busso, Maurizio, Palmerini, Sara, CRISTALLO, Sergio, Mengoni, Alberto, Simonucci, Stefano
Publisher's version (DOI)	10.3847/1538-4357/ac74b3
Handle	http://hdl.handle.net/20.500.12386/32972
Journal	THE ASTROPHYSICAL JOURNAL
Volume	933

The Astrophysical Journal, 933:158 (8pp), 2022 July 10 https://doi.org/10.3847/1538-4357/ac74b3

© 2022. The Author(s). Published by the American Astronomical Society.

OPEN ACCESS

Theoretical Estimate of the Half-life for the Radioactive ^{134}Cs and ^{135}Cs in Astrophysical Scenarios

Simone Taioli[1,2], Diego Vescovi[3], Maurizio Busso[4,5], Sara Palmerini[4,5,10], Sergio Cristallo[5,6],
Alberto Mengoni[7,8], and Stefano Simonucci[5,9]

[1] European Centre for Theoretical Studies in Nuclear Physics and Related Areas (ECT*), Bruno Kessler Foundation, Trento, Italy; taioli@ectstar.eu
[2] Trento Institute for Fundamental Physics and Applications (TIFPA-INFN), Trento, Italy
[3] Goethe University Frankfurt, Max-von-Laue-Strasse 1, Frankfurt am Main D-60438, Germany
[4] Department of Physics and Geology, University of Perugia, Via A. Pascoli snc, I-06123 Perugia, Italy
[5] INFN, section of Perugia, Via A. Pascoli snc, I-06123 Perugia, Italy; stefano.simonucci@unicam.it
[6] INAF, Osservatorio Astronomico d'Abruzzo, Via Mentore Maggini snc, I-64100 Collurania, Teramo, Italy
[7] ENEA, Dipartimento Fusione e Tecnologie per la Sicurezza Nucleare, Via Martiri di Monte Sole 4, I-40129 Bologna, Italy
[8] INFN, section of Bologna, Viale Berti Pichat 6/2, I-40127 Bologna, Italy
[9] School of Science and Technology, University of Camerino, Via Madonna delle Carceri 9B, I-62032 Camerino, Macerata, Italy
[10] INAF, Osservatorio Astronomico di Roma, Via Frascati, 33, 00078 Monte Porzio Catone, Rome, Italy

Received 2022 March 9; revised 2022 May 25; accepted 2022 May 28; published 2022 July 12

Abstract

We analyze the $^{134}_{55}\mathrm{Cs} \rightarrow ^{134}_{56}\mathrm{Ba}$ and $^{135}_{55}\mathrm{Cs} \rightarrow ^{135}_{56}\mathrm{Ba}$ β^- decays, which are crucial production channels for Ba isotopes in asymptotic giant branch (AGB) stars. We calculate, starting from relativistic quantum mechanics, the effects of multichannel scattering onto weak decays, including nuclear and electronic excited states (ESs) populated above $\simeq$10 keV, for both parent and daughter nuclei. We find increases in the half-lives for $T > 10^8$ K (by more than a factor of 3 for ^{134}Cs) as compared to previous works based on systematics. We also discuss our method in view of these previous calculations. An important impact on half-lives comes from nuclear ES decays, while including electronic temperatures yields further increases of about 20% at energies of 10–30 keV, typical of AGB stars of moderate mass ($M \lesssim 8\, M_\odot$). Despite properly considering these effects, the new rates remain sensitively lower than the Takahashi & Yokoi values, implying longer half-lives at least above 8–9 keV. Our rate predictions are in substantial accord with recent results based on the shell model, and strongly modify branching ratios along the *s*-process path previously adopted. With our new rate, nucleosynthesis models well account for the isotopic admixtures of Ba in presolar SiC grains and in the Sun.

Unified Astronomy Thesaurus concepts: S-process (1419); Nucleosynthesis (1131); Asymptotic giant branch stars (2100); Ionization (2068); Nuclear reaction cross sections (2087); Natural decay (2070)

1. Introduction

New scenarios to unravel heavy-element nucleosynthesis in stars were recently opened by extended surveys of spectroscopic observations (Ahumada et al. 2020), as well as by the analysis of presolar grains formed in stellar winds, which were trapped in pristine meteorites (Palmerini et al. 2021), offering new constraints on the isotopic abundances generated in stellar processes (Busso et al. 2021).

After decades of experiments on reaction rates for neutron captures and charged-particle processes, our understanding of the above scenario now depends also on improving the knowledge of weak nuclear reactions in hot stellar plasmas. Their accurate assessment still represents a crucial bottleneck, while experiments simulating stellar conditions in terrestrial ionized plasmas to measure decay rates are still in their infancy (Mascali et al. 2017, 2022). In particular, for a better agreement between nucleosynthesis models and observations (Vescovi et al. 2019) a great deal of theoretical work to assess stellar reaction rates with increased accuracy is still required (Nomoto et al. 2013); in fact, there is a dearth of computations for decay processes in stellar scenarios from first principles (Simonucci et al. 2013; Vescovi et al. 2019).

In this respect, we notice that β-decay spectra of allowed and forbidden transitions are typically calculated by using an analytical expression of the rate (Hayen et al. 2018), where semi-empirical factors account for the nuclear structure, the phase space, and the atomic exchange. However, not even this simpler approach is implemented in stellar neutron capture computations, where, instead, the phenomenological compilation (Takahashi & Yokoi 1983, 1987; hereafter TY) is universally used. There, unknown transition strengths are estimated by analogy to laboratory decays of nearby nuclei with similar transitions. In a recent study for example (Li et al. 2021), new $\log(ft)$ values were calculated from the nuclear shell model to obtain ^{134}Cs stellar rates within this standard approach (Hayen et al. 2018). In this work the electronic degree of freedom (DOF) is neglected, despite its crucial contribution to the rate. Nevertheless, the authors already show significant improvement in the astrophysical application, with the rate changing in the same direction as found using our analysis. Recently developed approaches, based on large-scale diagonalization shell model calculations, can be also used (Langanke et al. 2021), even though they have seen so far applications only to part of the nuclide chart.

One element requiring such studies is certainly barium. In asymptotic giant branch (AGB) stars, its abundance depends solely on slow (*s*) process nucleosynthesis that, after the *n*-capture on stable ^{133}Cs, meets a branching point at ^{134}Cs, where further *n*-captures compete with β-decay, e.g., the $^{134}_{55}\mathrm{Cs}(J^\pi = 4^+) \longrightarrow ^{134}_{56}\mathrm{Ba}(J^\pi = 4^+) + e^- + \bar{\nu}$ allowed

Original content from this work may be used under the terms of the Creative Commons Attribution 4.0 licence. Any further distribution of this work must maintain attribution to the author(s) and the title of the work, journal citation and DOI.

transition. Another reaction branching occurs at ^{135}Cs, β-decaying to ^{135}Ba via a second forbidden unique transition Cs $(7/2^+) \longrightarrow$ Ba$(3/2^+)$. The resulting balance, which should yield production of 100% of the *s*-only ^{134}Ba and ^{136}Ba isotopes, is thus very delicate. In particular, the ^{134}Cs $\longrightarrow ^{134}$Ba decay (half-life 2.0652 yr) is characterized by a *Q*-value (2058.7 keV; Sonzogni 2004) large enough to accommodate Cs high-lying nuclear excited states (ESs), e.g., 5^+ at 11.2442 keV and 3^+ at 60 keV above the ground state (GS). The emergence of ^{134}Cs short-lived nuclear ESs, possibly populated at high temperature, and the decay to ^{134}Ba isomers (such as 4^+, 3^+) may dramatically affect this transition owing to their different forbiddenness.

When *n*-capture on ^{134}Cs feeds the longer-lived ^{135}Cs, also the latter can decay through the mentioned Cs $(7/2^+) \longrightarrow$ Ba $(3/2^+)$ path. Its half-life is 2.3×10^6 yr (with a GS–GS *Q*-value of 268.7 keV; Singh et al. 2008). The inclusion of several ESs of ^{135}Cs (notably the $5/2^+$ states at 249.767 and 408.026 keV above the GS), together with the population of electronic excited levels, may significantly affect the total rate at high temperature also for this nucleus.

Furthermore, despite these transitions being quark-level processes, they also strongly depend on extra-nuclear factors, such as temperature and electron density, which significantly vary in the layers of evolved stars outside the degenerate core. Indeed, these parameters may affect the ionization degree of the atomic systems where the decay occurs, which in turn modifies the discrete-to-continuum transition ratio (Simonucci et al. 2013; Palmerini et al. 2016; Vescovi et al. 2019).

In this work we lay the foundation of a fully relativistic quantum mechanical method for calculating the temperature and density dependence of the β-decay half-life of *s*-process branching point isotopes, by considering both the electronic and nuclear ES population dynamics, and apply it here for the first time to ^{134}Cs and ^{135}Cs. We show that these DOFs act concurrently to strongly change the Cs isotopes half-lives, even by several orders of magnitude, with respect to laboratory conditions and previous phenomenological approaches based on systematics (see TY). We apply this approach to revise recent models aiming to explain the peculiar ratios of Ba isotopes in presolar SiC grains and the *s*-process origin of the ^{134}Ba and ^{136}Ba isotopes in the solar system (Palmerini et al. 2021; Busso et al. 2021).

2. Calculation of β-decay Rates of ^{134}Cs and ^{135}Cs

Our method is rooted in the single-particle mean-field (MF) approximation to the internuclear and interelectronic interactions, but is systematically and straightforwardly improvable by embedding higher accuracy many-body methods for including dynamical correlation (Hjorth-Jensen et al. 2017).

Our approach, based on the first-principle calculation of the transition operator written in terms of the total QED Hamiltonian, proved accurate in reproducing a few terrestrial observables (Morresi et al. 2018). Here, it is generalized to include the temperature and density dependence for dealing with astrophysical conditions (see Appendix A for further details). Within our framework, the weak Hamiltonian is factorized into the product of leptonic and hadronic currents (Morresi et al. 2018). We also require that the hadronic current is separable into neutron and proton field operators, which means essentially that the decaying neutron acts as a single particle correlated to the core of the remaining nucleons only geometrically, so as to recover the experimental total angular momentum of the parent reactant. Furthermore, one can safely assume that the leptonic current can be written as a product of the neutrino and electron quantum field operators. The hadronic and leptonic currents are both reckoned by the self-consistent numerical solution of the Dirac–Hartree–Fock equation (DHF).

Protons and neutrons interact via a semi-empirical relativistic Wood–Saxon potential, while the electron–electron Coulomb repulsion is modeled via a local density approximation to the electron gas ($V_{\rm ex} \propto \rho(r)^{1/3}$; Slater 1951; Salvat et al. 1987). Electrons populate the energy levels according to a Fermi–Dirac distribution, and the chemical potential is assessed by assuming that they behave as an ideal Fermi gas in a box with a relativistic energy-momentum dispersion. The non-orthogonality between the bound initial and final orbitals, the possible presence of shake-up (excitation) and shake-off (ejection) are also taken into account in the calculation of the continuum electron wave function. At high temperature, we considered positron formation, enforcing the overall neutrality of the plasma (see Table 3, which reports electron versus proton densities at all temperatures). For the $^{134}_{55}$Cs $\longrightarrow$ $^{134}_{56}$Ba transition, the lepton field carries no angular momentum. The rate has been assessed under the assumption, derived by the nuclear shell model, that the decaying neutron within the parent ^{134}Cs occupies the $2d_{3/2}$ shell, while the generated proton populates the $1g_{7/2}$ orbital of $^{134}_{56}$Ba. In principle, a superposition of single-particle nearby energy states mixed by the dynamical correlation, such as the ^{134}Cs $1h_{11/2}$ and $3s_{1/2}$ shells, may contribute to the β transition. However, owing to a bigger jump of ΔJ the level of forbiddenness of the β transition from those shells to the ^{134}Ba $1g_{7/2}$ shell would be higher and, thus, the transition less likely to occur.

In our calculations we included the 4^+ GS and the two lowest energy nuclear states (5^+, 3^+) of ^{134}Cs, occupied according to a Boltzmann distribution $f(E_i) = w_i e^{-E_i/K_{\rm B}T}$, where E_i is the energy of the *i*th nuclear level, weighted by the relevant level degeneration factor ($w_i = 9$, 11, and 7, respectively, for the three states mentioned above).

To reproduce the experimental values at Earth conditions, a constant correction factor of 4.4 to our calculated half-lives is applied at all temperatures. This renormalization factor is needed to correct the hadronic current, which may suffer from the MF evaluation of the nucleon wave functions. In our analysis we assume that the nuclear matrix elements do not depend on the temperature for a given transition because of the leptonic and hadronic currents factorization and of the independence of the single-particle orbitals of temperature. Indeed, the matrix elements of the hadronic currents only depend on the nuclear single-particle orbitals of the decaying neutron and of the proton before and after the decay, respectively. Once the initial parent and final daughter states are selected, the hadronic current matrix elements are independent of temperature, and their energy scale (MeV) is rather different from those typical of AGB stars (keV). In light of these considerations in place, we can safely state that the correction factor is the same at all temperatures and the fact that terrestrial decays are determined by decay of atomic Cs does not play any role. B

In Figure 1(a) and in the relevant inset, as well as in Table 1, we compare our results with those by TY. A finer grid of points can be found in Table 4 of Appendix B. We stress that in TY the effect of the excited nuclear dynamics on the β rates was estimated via the log(*ft*) values for general β transitions of

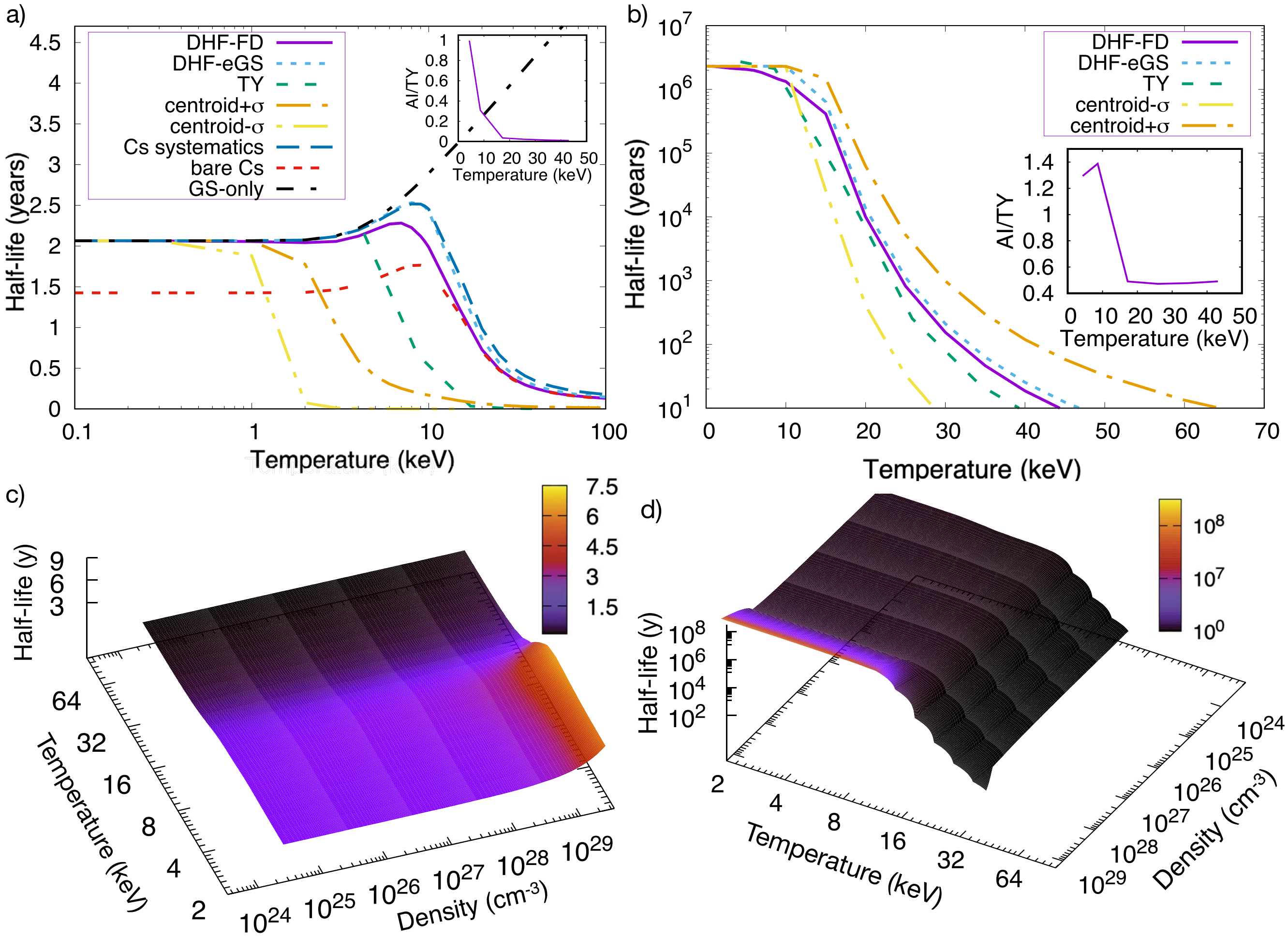

Figure 1. Half-life of ^{134}Cs (a) and of ^{135}Cs (b) vs. temperature (violet line) from our DHF calculations, for $n_p = 10^{26}$ cm^{-3}. They include: (a) the nuclear states at 4^+, 5^+, and 3^+ of ^{134}Cs and (b) those of ^{135}Cs at $5/2^+$, $5/2^+$, as well as the electronic DOF. In cyan (DHF-eGS) we show the half-life computed when electrons are clamped in their GS. Orange and yellow lines show the maximum (centroid$+\sigma$) and minimum (centroid$-\sigma$) values obtained by taking the log(*ft*) from the general systematics, while for the blue line we used simply the centroid of the specific ^{134}Cs systematics (this does not exist for ^{135}Cs). Green lines show the previous estimates by TY. In panel (a) we also show (red line) the half-life for a completely ionized ^{134}Cs (bare Cs) and the nuclear GS to GS decay half-life (black line, GS-only). The trend is similar for ^{135}Cs (not shown). Insets of (a) and (b) give the ratios between our ab-initio rates (AI) and TY values for $n_p = 10^{26}$ cm^{-3}. Panels (c) and (d) display ^{134}Cs and ^{135}Cs half-lives according to our model, including both nuclear and electronic DOFs, as a function of temperature and proton density.

Table 1
Comparison between TY ^{134}Cs Rates and Ours (in s^{-1} $\times$ 10^{-8}) for Different Temperatures and $n_p = 10^{26}$ cm^{-3}

T_8	TY	This Work
0.5 (4.31)	1.02	1.02
1 (8.62)	3.28	1.01
2 (17.23)	63.1	2.28
3 (25.85)	211.0	4.73
4 (34.47)	481.0	7.22
5 (43.09)	889.0	9.36

Note. Note that our rate remains always lower than those of TY. T_8 is the temperature expressed in 10^8 K, while the corresponding values in keV are in parentheses.

given forbiddenness derived from systematics. Moreover, at odds with our calculations, neither TY include in their estimate the electronic DOF, nor do they calculate the nuclear matrix elements from first principles.

We observe that the inclusion of the nuclear ES dynamics represents the most relevant effect on the ^{134}Cs β-decay rate at high temperatures (>10 keV), where nuclear states are most likely populated. Indeed, the presence of fast-decaying nuclear ESs can increase the rate by a factor of 15 at 100 keV (1 GK) and up to 23 at 1000 keV, with respect to room temperature conditions. In particular, such a half-life decrease can be almost entirely attributed to the 3^+ nuclear excited state (ES), which implies a rate 80 times higher than the 4^+ nuclear GS (if they were at each time the only occupied nuclear states to decay), while GS-only decay increases with temperature (as shown in Figure 1(a)).

We also notice that the temperature has a relevant effect on the lepton DOF in the range [0–10] keV, as revealed in Figure 1(a) by the difference between the full half-life and the one with electrons in their GS. In the case of a bare nucleus, where all Cs electrons are stripped out (the Cs 1*s* binding energy is 36 keV), the half-life is consistently lower (by 20% in laboratory conditions) than that of the neutral atom, as the emitted β-electron can land in any bound orbital. In Figure 1(a) we also report the reference band of the ^{134}Cs half-life using the standard deviation (centroid $\pm$ σ) of such systematics. We notice that TY recommendations are out of this range, while

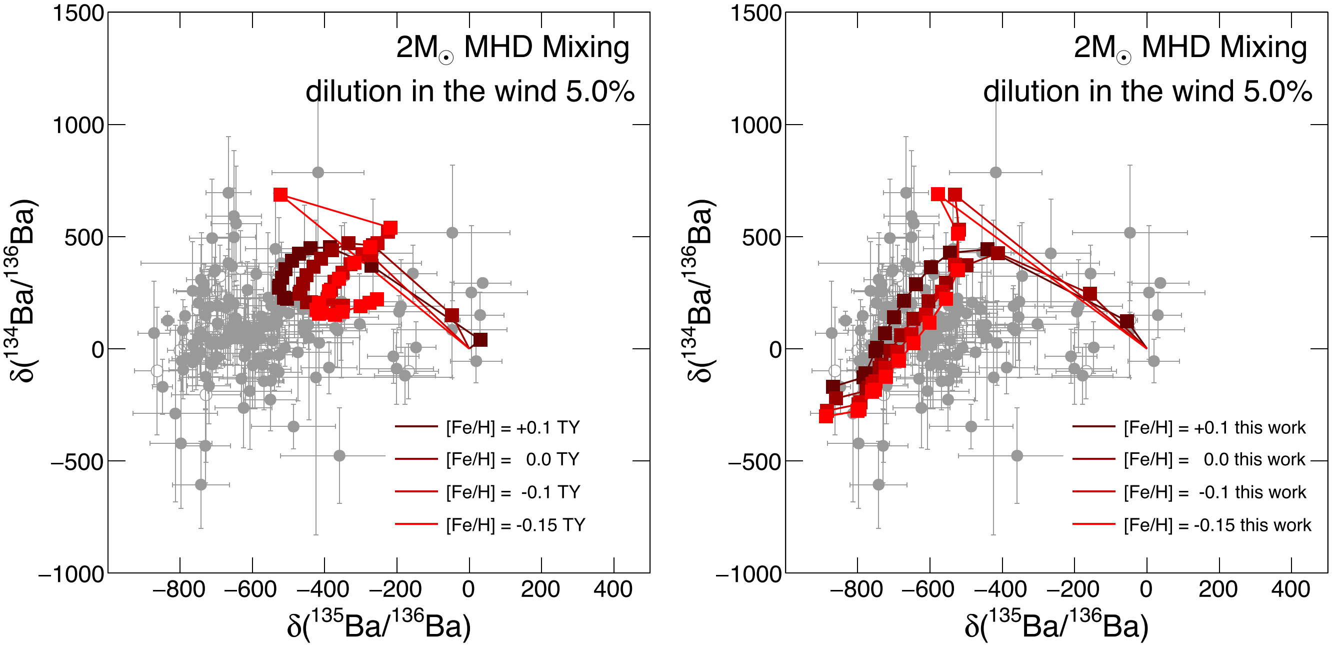

Figure 2. Left panel: isotopic ratios of ^{134}Ba and ^{135}Ba with respect to ^{136}Ba, displayed as part-per-mil deviations from the solar ratios (indicated by the symbol δ) computed in recent AGB models (Palmerini et al. 2021), with cross sections from the KADoNiS v1.0 database and decay rates from TY. Right panel: the results of the same models, where only the decay rates for ^{134}Cs and ^{135}Cs are changed, using those of the present work. We remind the reader that computations in Palmerini et al. (2021) are from 2 $M_\odot$ stars, where magnetohydrodynamic processes induce the penetration of protons into He-rich layers, producing ^{13}C and then releasing neutrons through $^{13}\mathrm{C}(\alpha, n)^{16}\mathrm{O}$. Abundances are computed in stellar winds, where we assume that magnetic blobs further add 5% of *s*-process rich material in flare-like episodes. The symbol [Fe/H] indicates $\log(X_{\mathrm{Fe}}/X_{\mathrm{H}})_{\mathrm{star}} - \log(X_{\mathrm{Fe}}/X_{\mathrm{H}})_{\mathrm{sun}}$. Curves with different colors refer to stellar models of different metallicity.

Table 2
Comparison between TY ^{135}Cs Rates and Ours (in s^{-1}) for Different Temperatures and Proton Densities

	$n_p = 10^{26}$ cm^{-3}		$n_p = 3\times10^{26}$ cm^{-3}		$n_p = 10^{27}$ cm^{-3}		$n_p = 3\times10^{27}$ cm^{-3}	
T_8	TY	This Work	TY	This Work	TY	This Work	TY	This Work
0.5 (4.31)	8.12e-15	1.05e-14	7.90e-15	1.02e-14	7.92e-15	9.70e-15	7.39e-15	9.11e-15
1 (8.62)	1.04e-14	1.44e-14	8.78e-15	1.22e-14	8.04e-15	1.08e-14	7.81e-15	9.79e-15
2 (17.23)	6.91e-13	3.39e-13	6.65e-13	3.27e-13	6.09e-13	3.01e-13	5.52e-13	2.66e-13
3 (25.85)	8.64e-11	4.08e-11	8.55e-11	4.04e-11	8.24e-11	3.91e-11	7.74e-11	3.64e-11
4 (34.47)	9.77e-10	4.66e-10	9.65e-10	4.64e-10	9.52e-10	4.57e-10	9.17e-10	4.38e-10
5 (43.09)	4.18e-09	2.05e-09	4.15e-09	2.05e-09	4.08e-09	2.03e-09	3.96e-09	1.97e-09

Note. Both our rates are lower than those of TY at $T > 10^8$ K. T_8 is the temperature expressed in 10^8 K, while the corresponding values in keV are in parentheses.

our results are in better agreement with the specific systematics of ^{134}Cs (where the electronic DOF are of course neglected).

Finally, in Figure 1(c) we plot the ^{134}Cs half-life versus proton density and temperature as varying in the interior of stars. We notice that, at temperatures >10 keV, the half-life shows a significant drop, even at very high density, owing to the decay from the ^{134}Cs nuclear ESs.

A similar analysis has been carried out also for the ^{135}Cs β-decay. In Figure 1(b) we plot the half-life versus temperature obtained by our DHF model as compared to TY estimates (color codes are explained in the caption). To reproduce the experimental values at Earth conditions, a constant correction factor of ≈90 to our calculated half-lives is applied at all temperatures. The half-lives of both ^{134}Cs and ^{135}Cs with and without the correction factors are reported in Table 6 of Appendix B. In this case, both data sets are found within the range spanned by the general systematics for these transitions. Again, we plot the half-life obtained with electrons clamped in their GS to determine the electronic contribution to the β transition with increasing temperature. The latter is neglected in TY, while the inclusion of this DOF may almost halve the half-life around 10 keV. The results obtained with our model are compared with those of TY in Table 2 and in the inset of Figure 1(b); (a finer grid is reported in Table 5 of Appendix B). In Figure 1(d) we report the half-life versus temperature and proton density, finding a similar but steeper descent with increasing temperature with respect to ^{134}Cs.

3. Astrophysical Implications and Conclusions

Our results immediately confirm recent suggestions (Busso et al. 2021), according to which a more accurate treatment of β-decays in hot plasmas is needed for improving the modeling of Ba isotopes in AGB stars. This is especially true for the composition of presolar SiC grains (Palmerini et al. 2021). We therefore used our rates to revise the calculations presented in Palmerini et al. (2021). In Figure 2 (left panel) we present the results obtained by using cross sections from the KADoNiS repository (Karlsruhe Astrophysical Database of

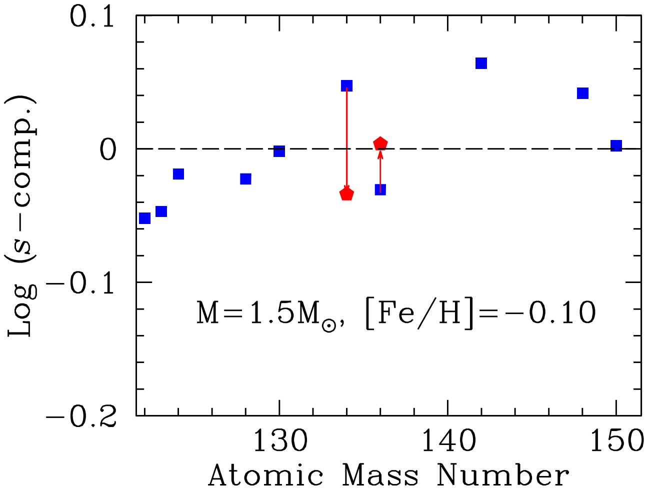

Figure 3. Percentage of s-process contributions (blue dots) as computed by Busso et al. (2021) for s-only nuclei near the magic neutron number $N = 82$. In a perfect model, without nuclear or stellar uncertainties, all points should be aligned at zero. Red points (marked by arrows) show the results for ^{134}Ba and ^{136}Ba in a revised calculation where, all the rest remaining the same, we adopted the β^--decay rates for ^{134}Cs and ^{135}Cs computed in the present work. We note that two more nuclei look to be outliers in the figure. They are ^{142}Nd and ^{148}Sm, whose abundances are critically linked to the decay rates of ^{142}Pr, ^{147}Nd, and ^{148}Pm, for which a revision like the present one would be needed.

Nucleosynthesis in Stars version v1.0; Dillmann et al. 2014) and decay rates from TY. The right panel shows the changes obtained exclusively by adopting the β-decay rates of this work. We stress that the new model curves, reproducing the expectations of AGB stars characterized by masses and metallicities as indicated, improve remarkably the agreement with observational constraints (gray dots) and fit well the main area occupied by the data. We notice that the novel rates presented here improve even on a tentative guess reported in Palmerini et al. (2021; see Figure 19(a) therein).

An additional implication of our half-life revision concerns the solar distribution of s-elements. In this regard, very recently rather extensive analyses of neutron captures in AGB stars pointed out that a reappraisal of the rates here presented for β^- decays, with a more accurate treatment of their dependence on temperature and density, was crucial for any improvement in our understanding of the isotopic admixture of Ba in the Sun (Busso et al. 2021). In particular, it was shown that (see Figure 4 in Busso et al. 2021) an average model could be identified, suitable to mimic (if properly normalized) the outcomes of a simulation from a chemical evolution model of the Galaxy at least for the s-process contribution to heavy nuclei. In those estimates, ^{134}Ba and ^{136}Ba should be both at the level of one, as they do not receive contributions from other processes. In Figure 3 we show the results of the calculations carried out using the same physical models and nuclear parameters as in Busso et al. (2021), only updating the two rates discussed here. The percentage of s-process contributions to the isotope production is plotted in log scale (thus for $\log(s) = 0$ the contribution is s-only). With blue dots we show the original results for s-only nuclei sited close to the magic neutron number $N = 82$. In red we report the new values found for ^{134}Ba and ^{136}Ba using our new rates (all the rest remaining untouched). We stress that the improvement over the previous expectations is striking. We notice that similar improvements are also expected for Galactic chemical evolution models computed with full stellar evolutionary yields (Prantzos et al. 2020), which were showed to have severe problems with ^{134}Ba and ^{136}Ba.

In conclusion, we find that the β-decay rates of the ^{134}Cs and ^{135}Cs isotopes remain lower (even by large factors for ^{134}Cs) than the widely used TY estimates, thus pointing to longer half-lives at temperatures $T > 10^8$ K, which characterize the regions of the AGB stars where the s-process nucleosynthesis occurs. This condition applies to both Cs isotopes even after considering that the rates are dramatically increased at high temperature by two concurrent factors: the inclusion of both the nuclear and the electronic ESs of parent and daughter nuclei, up to complete ionization. Most notably: (i) the 60 keV nuclear ES of ^{134}Cs, while scarcely populated, is the fastest to β-decay, with a rate $\simeq$80 times higher than the GS–GS one; (ii) the rate increases with respect to GS decay only, close to a factor of $\simeq$3 at 20 keV, $\simeq$6 at 30 keV, and $\simeq$8 at 40 keV. For ^{135}Cs similar effects, concurrent in lowering the half-life, were found, and our results are within the standard deviation of the general systematics.

The use of the new rates to s-process computations in AGB stars remarkably reconciles models and observations for both the Sun and the presolar SiC grain isotopic composition by leading to an overall decrease in the ^{134}Ba/^{136}Ba and ^{135}Ba/^{136}Ba abundance ratios predictions, and provides realistic inputs and comparisons to the now forthcoming experiments (Mascali et al. 2017, 2022).

D.V. acknowledges financial support from the German-Israeli Foundation (GIF No. I-1500-303.7/2019).

Appendix A
Theoretical and Computational Model

Here, we recap a few mathematical and computational details of our method for calculating β-decay in astrophysical scenarios. In the traditional approach, β-decay spectra of allowed and forbidden transitions are calculated by using an analytical expression of the rate (Hayen et al. 2018) where several factors appear that account for the nuclear and phase-space structure and for the atomic exchange. Instead, our approach is based on the calculation of the total Hamiltonian of the system:

$$\mathcal{H} = \mathcal{H}_{\text{nucl}} + \mathcal{H}_{\text{e-e}} + \mathcal{H}_{\text{weak}}, \tag{A1}$$

where $\mathcal{H}_{\text{nucl}}$ contains the interactions between nucleons in the initial and final nuclear states, $\mathcal{H}_{\text{e-e}}$ is the electron–electron Coulomb correlation, taking into account that the transition occurs inside a partially ionized atom, and finally $\mathcal{H}_{\text{weak}}$ is the zero-order QED weak interaction, which fulfills the Lorentz invariance:

$$\mathcal{H}_{\text{weak}} = \frac{G_F}{\sqrt{2}} H_\mu L^\mu + \text{h.c.} \tag{A2}$$

Here, $G_F = 1.16637 \times 10^{-5}$ GeV^{-2}, L^μ is the lepton current,

$$L^\mu = \bar{u}_e \gamma^\mu (1 - \gamma^5) v_\nu, \tag{A3}$$

and H_μ is the hadronic current,

$$H_\mu = \bar{u}_p \gamma_\mu (1 - x\gamma^5) v_n. \tag{A4}$$

In Equations (A3)–(A4) γ^μ, $\mu = 0, \ldots, 4$ are the Dirac matrices, x is the ratio between the axial vector coupling constant c_A and the vector coupling constant c_V, $\frac{c_A}{c_V} \sim 1.2756$, and u_e, v_ν, v_n, and u_p are the β-electron, neutrino, neutron, and proton annihilation operators, respectively.

In particular, we are interested in reckoning the probability per unit time that the atomic system decays from a statistical mixture of initial states $\hat{\rho}_i = p_i|i><i|$ to a mixture of final states $P_f = \sum_f |f><f|$, that is:

$$N_{i\to f} = 2\pi\,\mathrm{Tr}(\hat{\rho}_i \mathcal{H}_{\mathrm{weak}} P_f \mathcal{H}_{\mathrm{weak}})\delta(E_i - E_f) + h.c. \qquad \text{(A5)}$$

In the typical approximation to the general theory of β-decay, where the recoil energy of the final nucleus is small with respect to the nucleon rest mass, the initial and final states can be written as:

$$|i\rangle = |h_i\rangle \otimes |e_i\rangle \qquad \text{(A6)}$$

$$|f\rangle = |h_f\rangle \otimes |e_f\rangle \otimes |\bar{\nu}_f\rangle, \qquad \text{(A7)}$$

where $|h_{(i,f)}\rangle$ are initial and final multi-nucleon states characterized by the quantum numbers $|J_{(i,f)}, M_{(i,f)}, T_{(i,f)}\rangle_{\mathrm{nucl}}$, where $J_{(i,f)}$ and $M_{(i,f)}$ denote the total angular momentum and its projection along some fixed axis of the initial and final states, respectively, and $T_{(i,f)}$ is the isospin; $|e_i\rangle = |j_i, m_i; [n_1^b \cdots n_k^b]_{(i)}\rangle_{\mathrm{e-e}}$ is the initial many-electron state, where $[n_1^b \cdots n_k^b]_{(i,f)}$ represent the bound orbitals; finally, $|\bar{\nu}_f\rangle$ is the final anti-neutrino state (typically represented by a free plane wave).

We point out that the initial and final multi-nucleon states and the initial multi-electron states are characterized by a discrete spectrum, while the final multi-electron state, which describes the β emission, is a continuum state that can be written as a linear combination of external products $|e_f> = \sum_j I_{j,f} \wedge |\eta_{j,f}>$, where $|\eta_{j,f}>$ describes the β-electron continuum wave function and $I_{j,f}$ represents the final bound state.

Within this framework, the evaluation of the transition operator can be factorized into the product of lepton and hadronic currents (Morresi et al. 2018). This is ultimately due to the large rest mass of the W vector boson that mediates the weak interaction. Furthermore, we can safely assume that electrons and neutrinos are not coupled and thus the lepton current (A3) can be further factorized in the independent product of the neutrino and electron quantum field operators (or, dealing with expectation values, wave functions). In this work, we also make the assumption that the hadronic current can be factorized in the product of neutron and proton field operators. The hadronic current separability is basically equivalent to the requirement that only one nucleon within the parent nucleus participates into the decay dynamics. The decaying nucleon is thus an independent particle, uncorrelated to the "core" of the remaining nucleons. Such a core, which couples only geometrically to the decaying nucleon so as to recover the total angular momentum of the parent reactant and of the final daughter nucleus, is approximated by a linear combination of angular momentum wave functions. Our approximation assumes the validity of the nuclear shell model. However, this does not represent an intrinsic limit of our method, as the hadronic current for systems where many-body effects are expected to play a paramount role can be assessed separately, via more accurate first-principle approaches (Hjorth-Jensen et al. 2017). The hadronic current (A4) is derived by an explicit numerical solution of the Dirac equation (DE) in a central potential. In our solution, protons and neutrons interact via a semi-empirical scalar and vector relativistic Wood–Saxon (WS) spherical symmetric potential, which describes the nucleon–nucleon interaction (Schwierz et al. 2007), whereby the DE is monodimensional in the radial variable. To solve the equation, a grid with a few thousands points is used (Morresi et al. 2018).

Table 3
The n_e/n_p and $(n_e - n_p)/n_p$ Ratios as a Function of Temperature T (keV)

	$n_p = 10^{26}$		$n_p = 10^{27}$	
T	n_e/n_p	$(n_e - n_p)/n_p$	n_e/n_p	$(n_e - n_p)/n_p$
10	1.0	0.0	1.0	0.0
20	1.0	2.121e-18	1.0	2.234e-21
30	1.0	2.381e-10	1.0	2.57342e-13
40	1.0	2.5098e-06	1.0	2.74123e-09
50	1.0009	0.00087	1.0	9.5167e-07
60	1.0460	0.0460	1.00005	5.3074e-05
70	1.5858	0.5858	1.001025	0.001025
80	3.5663	2.5663	1.010026	0.010026
90	8.0831	7.0831	1.0599	0.05987
100	16.61334	15.61334	1.2334	0.2333676

Also the electron wave functions are found by solving self-consistently the Dirac–Hartree–Fock (DHF) equation in a central potential. Electrons interact via a mean field, where the nonlocal exchange (Fock term) is replaced by the local density approximation (LDA) to the electron gas ($V_{ex} \propto \rho(r)^{1/3}$; Slater 1951; Salvat et al. 1987). The numerical solution of the DHF equation was found by using a modified Runge–Kutta method (Morresi et al. 2018). The non-orthogonality between the bound initial n_i^b and final n_f^b orbitals, which are obtained by solving the DHF equations for the parent and daughter nuclei carrying a different atomic number, is taken into account. The continuum β-electron wave function $\psi_{f,e}^c(\boldsymbol{r})$ is then expressed in the field produced by both the nucleus and the surrounding electrons as a Slater determinant, to take into account the atomic exchange. The β-electron continuum wave function within this framework thus reflects the fact that the emitted lepton may decay into a bound state of the daughter nucleus with ejection of a secondary bound electron and that final state excitations, such as shake-up and shake-off (Morresi et al. 2018), can be present. Atomic exchange effects open up multiple decay channels that typically increase the β-decay rate particularly at low energies (Harston & Pyper 1992), where the overlap between the continuum and discrete wave functions maximizes.

Electrons populate the energy levels according to a Fermi–Dirac (FD) distribution $n_{e^-}^i = \frac{1}{1 + e^{(\epsilon_i - \mu_{e^-})/(K_{\mathrm{B}}T)}} = F(T, \mu_{e^-})$, where K_{B} is the Boltzmann constant and T is the temperature. The eigenvalues ϵ_i are obtained by a self-consistent solution of the DHF equation for the leptons, and the chemical potential is assessed by assuming that the electrons behave as an ideal Fermi gas in a box with a relativistic energy-momentum dispersion $E^2 = c^2p^2 + m_e^2c^4$ as $n_{e^-} = \int_0^\infty dp\, p^2/\pi^2 \times (F((c \times \sqrt{(}p^2 + m_e^2c^2) - \mu_e)/K_{\mathrm{B}}T) - F((c \times \sqrt{(}p^2 + m_e^2c^2) + \mu_e)/K_{\mathrm{B}}T))$. We notice that the electron orbitals of Cs and Ba have not been reoptimized at each temperature. At very high temperatures, however, we included positron formation in our model. The plasma at a given temperature is assumed to be overall neutral, that is $n_p = n_{e^-} - n_{e^+}$, where n_p, n_{e^-}, n_{e^+} are the proton, electron, and positron density, respectively. Note that $n_p \approx n_{e^-}$ at high densities, while they can differ sensibly a low densities. Protons are treated as nonrelativistic particles and their density has been varied in the range $n_p = 10^{24}$–10^{27} to model different astrophysical scenarios. In Table 3 we report the proton versus relevant electron densities at different temperatures.

Appendix B
Half-life Tables

In Tables 4 and 5 we report the half-lives of ^{134}Cs and ^{135}Cs on a finer mesh. In Table 6 we report the same half-lives at Earth conditions compared to experimental data.

Table 4

^{134}Cs Half-lives (yr) Obtained for Several Densities (cm^{-3}) and Temperatures T (keV)

T	n_p					
	6×10^{24}	6×10^{25}	6×10^{26}	6×10^{27}	6×10^{28}	6×10^{29}
0.86	2.04149	2.05406	2.07755	2.15924	2.55484	5.56986
1.085	2.03336	2.05026	2.07621	2.15899	2.5548	5.56984
1.37	2.01435	2.04481	2.07446	2.15896	2.55518	5.57079
1.719	1.9947	2.03652	2.07328	2.16047	2.55763	5.57629
2.16	1.98896	2.02753	2.07546	2.16711	2.56659	5.59606
2.725	2.00225	2.02915	2.08667	2.18582	2.59062	5.64877
3.43	2.03635	2.05478	2.11409	2.2243	2.63937	5.75549
4.319	2.07298	2.10883	2.16471	2.2886	2.72088	5.93362
5.44	2.00961	2.17161	2.23866	2.37687	2.83378	6.1752
6.845	1.86683	2.1586	2.30543	2.46085	2.94249	6.35983
8.62	1.78273	1.97719	2.24599	2.43095	2.90337	6.01333
10.85	1.58026	1.64867	1.87921	2.08555	2.4593	4.55354
13.66	1.17738	1.19422	1.29305	1.45373	1.67893	2.70035
17.19	0.765335	0.769108	0.798542	0.886004	1.00964	1.47377
21.65	0.48386	0.484805	0.493239	0.533676	0.606594	0.84334
27.25	0.321219	0.321509	0.324257	0.342418	0.389374	0.530591
34.31	0.228839	0.228947	0.229995	0.238386	0.269924	0.365959
43.19	0.174786	0.174833	0.175296	0.179417	0.200815	0.27283
54.37	0.141613	0.141634	0.141865	0.144038	0.158478	0.215895
68.453	0.120307	0.120315	0.120432	0.121659	0.131326	0.178361
86.17	0.106109	0.106113	0.106165	0.106871	0.113322	0.151812

Table 5

The ^{135}Cs Half-lives (yr) Obtained for Several Densities (cm^{-3}) and Temperatures T (keV)

T	n_p					
	6×10^{24}	6×10^{25}	6×10^{26}	6×10^{27}	6×10^{28}	6×10^{29}
0.86	2.24735e+06	2.28314e+06	2.35169e+06	2.5949e+06	4.05442e+06	1.38295e+08
1.085	2.22363e+06	2.27205e+06	2.34741e+06	2.59384e+06	4.05376e+06	1.38122e+08
1.37	2.16957e+06	2.25504e+06	2.3407e+06	2.59214e+06	4.05272e+06	1.37847e+08
1.719	2.11206e+06	2.22521e+06	2.33048e+06	2.58945e+06	4.05111e+06	1.37424e+0
2.16	2.07881e+06	2.17983e+06	2.31431e+06	2.58509e+06	4.04856e+06	1.36759e+08
2.725	2.06411e+06	2.1325e+06	2.28881e+06	2.57781e+06	4.04444e+06	1.35701e+08
3.43	2.0522e+06	2.09846e+06	2.25322e+06	2.56603e+06	4.03796e+06	1.34072e+08
4.319	1.97606e+06	2.07086e+06	2.21036e+06	2.54721e+06	4.02766e+06	1.3157e+08
5.44	1.62748e+06	1.9987e+06	2.16292e+06	2.51833e+06	4.01129e+06	1.27794e+08
6.845	1.24302e+06	1.75501e+06	2.09403e+06	2.47574e+06	3.9854e+06	1.22285e+08
8.62	1.10909e+06	1.39724e+06	1.94529e+06	2.41137e+06	3.94404e+06	1.14477e+08
10.85	1.07248e+06	1.18395e+06	1.67416e+06	2.29764e+06	3.85507e+06	9.81098e+07
13.66	806399	834310	1.02279e+06	1.44121e+06	2.24393e+06	1.27362e+07
17.19	72041.5	72659.3	77637.2	94275.4	123468	340712
21.65	3851.17	3865.52	3995.78	4683.27	6254.44	16801.2
27.25	358.829	359.506	365.995	412.098	563.022	1513.15
34.31	53.6033	53.6588	54.2028	58.7768	80.1084	214.686
43.19	11.6125	11.6195	11.6889	12.3265	16.2948	42.9303
54.37	3.34727	3.34841	3.36067	3.47855	4.37922	11.0515
68.453	1.20894	1.20911	1.2117	1.23923	1.47913	3.46087
86.17	0.527193	0.527237	0.527765	0.535284	0.609228	1.28288

Table 6
The ^{134}Cs and ^{135}Cs Half-lives (yr) at Earth Conditions Compared to Experimental Data (Obs.)

	Obs.	wcf
^{134}Cs	2.0652	8.80
^{135}Cs	2.3e+06	0.025e+06

Note. The half-lives obtained by our model are given here without the correction factor (wcf). The correction factors to reproduce the measured half-lives are 4.4 and ≈90 for ^{134}Cs and ^{135}Cs, respectively.

ORCID iDs

Simone Taioli https://orcid.org/0000-0003-4010-8000
Diego Vescovi https://orcid.org/0000-0003-0309-4666
Maurizio Busso https://orcid.org/0000-0001-8944-5820
Sara Palmerini https://orcid.org/0000-0001-5386-8389
Sergio Cristallo https://orcid.org/0000-0001-9683-9406
Alberto Mengoni https://orcid.org/0000-0002-2537-0038
Stefano Simonucci https://orcid.org/0000-0001-9287-8651

References

Ahumada, R., Prieto, C. A., Almeida, A., et al. 2020, ApJS, 249, 3
Busso, M., Vescovi, D., Palmerini, S., Cristallo, S., & Antonuccio-Delogu, V. 2021, ApJ, 908, 55
Dillmann, I., Szücs, T., Plag, R., et al. 2014, NDS, 120, 171
Harston, M. R., & Pyper, N. C. 1992, PhRvA, 45, 6282
Hayen, L., Severijns, N., Bodek, K., Rozpedzik, D., & Mougeot, X. 2018, RvMP, 90, 015008
Hjorth-Jensen, M., Lombardo, M. P., & van Kolck, U. (ed.) 2017, An Advanced Course in Computational Nuclear Physics, Vol. 936 (Berlin: Springer)
Langanke, K., Martínez-Pinedo, G., & Zegers, R. G. T. 2021, RPPh, 84, 066301
Li, K.-A., Qi, C., Lugaro, M., et al. 2021, ApJL, 919, L19
Mascali, D., Musumarra, A., Leone, F., et al. 2017, EPJA, 53, 145
Mascali, D., Santonocito, D., Amaducci, S., et al. 2022, Univ, 8, 80
Morresi, T., Taioli, S., & Simonucci, S. 2018, Advanced Theory and Simulations, 1, 1870030
Nomoto, K., Kobayashi, C., & Tominaga, N. 2013, ARA&A, 51, 457
Palmerini, S., Busso, M., Simonucci, S., & Taioli, S. 2016, JPhCS, 665, 012014
Palmerini, S., Busso, M., Vescovi, D., et al. 2021, ApJ, 921, 7
Prantzos, N., Abia, C., Cristallo, S., Limongi, M., & Chieffi, A. 2020, MNRAS, 491, 1832
Salvat, F., Martìnez, J. D., Mayol, R., & Parellada, J. 1987, PhRvA, 36 467
Schwierz, N., Wiedenhover, I., & Volya, A. 2007, arXiv:0709.3525
Simonucci, S., Taioli, S., Palmerini, S., & Busso, M. 2013, ApJ, 764 118
Singh, B., Rodionov, A. A., & Khazov, Y. L. 2008, NDS, 109, 517
Slater, J. C. 1951, PhRv, 81, 385
Sonzogni, A. 2004, NDS, 103, 1
Takahashi, K., & Yokoi, K. 1983, NuPhA, 404, 578
Takahashi, K., & Yokoi, K. 1987, ADNDT, 36, 375
Vescovi, D., Piersanti, L., Cristallo, S., et al. 2019, A&A, 623, 7